CHAPTER 157

MODELLING THE IMPACT OF DETACHED BREAKWATERS ON THE COAST

K.J. Bos[1], J.A. Roelvink[1] and M.W. Dingemans[1]

1. Introduction

Detached breakwaters alter the nearshore wave climate and hence the wave-driven current and sediment transport patterns. They obstruct a part or all of the longshore sediment transport and because of this they play a role in the large-scale sediment budget of the coasts where they are applied. Their local effect on the coast is to form single or double salients or tombolos. Which of these beach shapes will develop may be important for the attractiveness of the beach, in terms of visual aspects and water quality.
Besides having a function as part of a coastal management scheme, detached breakwaters with a jetty to the shore may be designed as a low-maintenance port. Obviously, one hopes that in such cases a salient rather than a tombolo will develop.
Clearly, engineers need to have means to assess the bypass-characteristics and the local impact of detached breakwaters if they want to apply them in a responsible manner. Several methods are at their disposal.
First, there are rules-of-thumb, based on field and lab experience. These are quite useful to get a first rough idea of the possible impacts, but generally do not give answers that are conclusive enough: a typical result is of the form that two design rules say you'll get a salient and three say you'll get a tombolo.
The most common tools applied at present are coastline models. They assume that the coastal profile is more or less constant in shape, and that the longshore sediment transport is related to the local angle of incidence of the waves. Several commercially available packages have special options to assess the local wave climate behind detached breakwaters. Effects that are not included in the current and transport models, such as circulations induced by set-up gradients, can be simulated by adjusting transport parameters locally. Generally, a lot of calibration is required, and the predictive capability is often uncertain. The calibrated models often show nice comparisons with data, especially for the initial stages. The development towards equilibrium is generally not represented at all.
Recently, more sophisticated "area models" have matured to the point that fully dynamic wave, current, transport and bed evolution simulations can be carried out over a period which is long enough to approach equilibrium conditions (see for instance Johnson et al., 1994). The advantages are obvious: these models explicitly take into account the most important processes, and therefore the amount of heuristic modelling is reduced substantially.

In the light of the ongoing efforts of devising coastal area morphological models, the performance of DELFT HYDRAULICS morphological model is tested on the simple situation of a detached breakwater in a coastal area with parallel iso-baths. This also furnishes a test for the DELFT3D system and has proven an opportunity of improving the model.

Netherlands Centre for Coastal Research (NCK), Delft University of Technology, c/o DELFT HYDRAULICS, PO Box 177, 2600 MH Delft, the Netherlands.

2. The model

The model system which is tested is DELFT HYDRAULICS morphological model DELFT3D. This model allows a flexible integration of the models for currents, waves, sediment transport, bottom changes, water quality and ecology (Roelvink and Van Banning, 1994; Roelvink et al., 1995). The morphological system contains the first four models and a control model. This control model allows the user to prescribe any combination of processes and arranges the time-progress of each model and possible iterations between models. The models relevant to morphological simulations are outlined below:

waves
Stationary multi-directional (short-crested) wave model HISWA (Holthuijsen et al., 1989). The model solves the spectral wave action balance equation assuming a frequency spectrum of fixed shape. The model includes directional spreading, wave shoaling, refraction, dissipation by bottom friction and wave breaking, current refraction and wave blocking.

Hydrodynamics
2D or 3D flow model DELFT3D-FLOW (formulae TRISULA) based on the shallow water equations, including effects of tides, wind, density currents, waves, spiral motion and turbulence models up to k-ε; for morphodynamic computations, a quasi-3D option to account for wave-driven cross-shore currents is available.

Sediment transport
The sediment transport can be calculated according to several formulae, including bed-load and suspended load transport. Typical cross-shore effects such as return flow and wave asymmetry can be accounted for. The model includes a quasi-three-dimensional advection diffusion solver for suspended sediment, including temporal and spatial lag effects.

Bottom change
The bottom changes are computed from the sediment mass continuity equation. This equation is solved with a forward-time, central space (FTCS) explicit numerical scheme. The model contains a built-in time step optimization procedure.

The flow diagram for the combination of models applied in this study is given in Figure 1. Starting from an initial bathymetry, a wave computation is carried out followed by a run of the flow model. The wave and current computation can be iterated to account for full wave-current interaction. Sediment transport computations are carried out for a number of steps. After each step the bathymetry is updated based on the residual transport pattern. A very important branch in this scheme is denoted by B. Here, the discharge pattern is kept constant and (small) bottom changes are assumed to affect the current only locally: at a constant discharge rate, the current velocity increases if depth decreases. This is a reasonable assumption as long as the bottom changes are small and lead to an enormous reduction in computational cost. Typically, 20-40 so-called continuity correction steps can be taken in between full hydrodynamic runs (branch A).
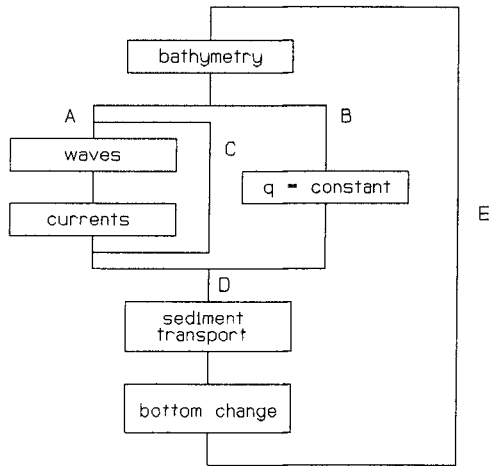
Figure 1   Flow diagram of morphological model system.

3. Test case

The breakwater lay-out to be simulated exists of a single offshore breakwater placed on a plane sloping 1:50 beach profile. The breakwater has a length of 300 m and is subjected to the action of normal or oblique incident storm waves, H_{rms} = 2.00 m. The relevant parameters are summarized below:

breakwater lay-out
beach slope	= 1:50	
L_b	= 300 m	breakwater length
X_b	= 220 m	breakwater axis-to-shore distance
h_b	= 4.6 m	depth at the seaward side of the breakwater

wave data
H_{rms}	= 2.0 m	root mean square wave height
T_p	= 8.0 s	peak wave period
θ	= 0° or 30°	mean wave direction

hydrodynamic data
tide	= absent

sediment data
ρ	= 2650 kg/m³	mass density of sediment
d_{50}	= 250 μm	median diameter
ϵ	= 0.4	porosity of sediment

4. 2DH results

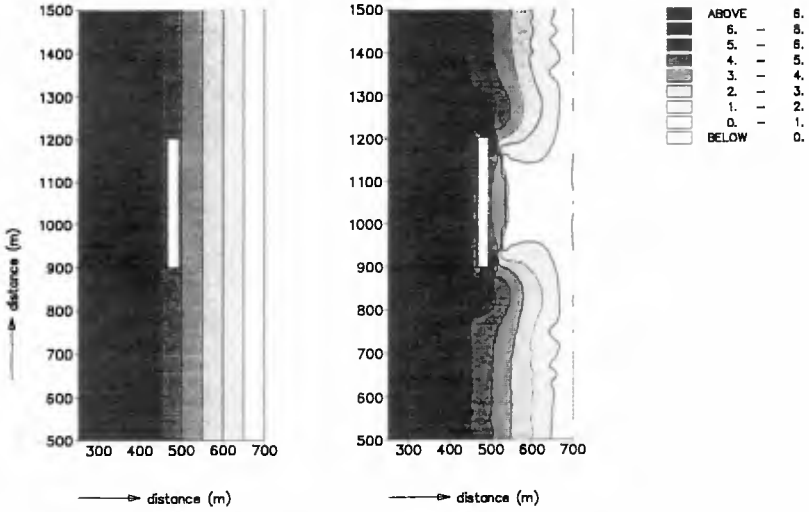Within the 2DH computations the transport formula of Bijker is used.

Figure 2 Left: Initial bathymetry; right: Bathymetry after 200 hours.

Normal incident waves

In the left part of Figure 2 the initial bathymetry is shown. In Figure 3 the initial wave pattern, water level and flow field are presented for normal incident waves.
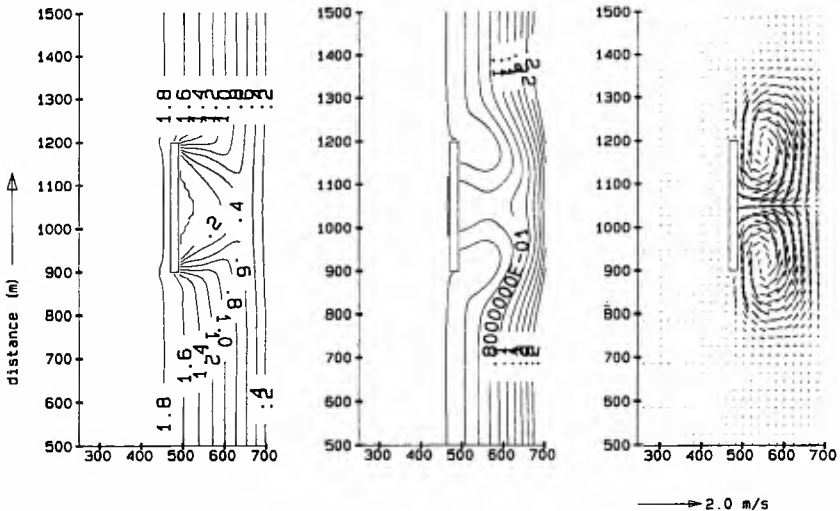

Figure 3 Left: Initial wave pattern; middle: Initial water level; right: Initial flow pattern.

The waves penetrate into the sheltered area as a result of diffraction. Although wave diffraction is not accounted for in HISWA its effect is limited in view of the wide directional

COASTAL ENGINEERING 1996

spreading used. Comparison of HISWA and a parabolic model by DHI (Johnson et al., 1994) showed that HISWA yields less wave activity and induced current behind the breakwater. However, these differences are partly due to the directional spreading accounted for in HISWA (and not in the parabolic model) since directional spreading has a smoothing effect on the wave and current field.

The isolines plot of the wave height shows that the breakwater is place in the breaker zone which extends over about 300 m. As a result of the difference in wave height in longshore direction a water level gradient is present which generates two circulatory cells in the lee of the breakwater. These gyres have high current velocities up to 0.88 m/s at the breakwater tips which are able to transport sediment towards the lee of the breakwater (Figure 4).
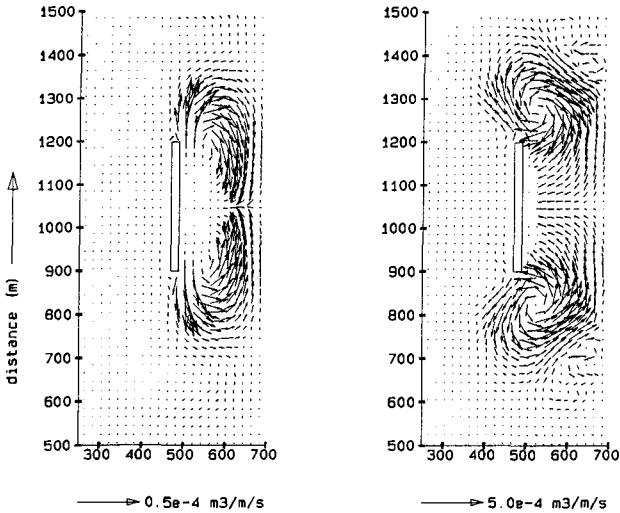

Figure 4 Left: Initial sediment transport pattern; right: Sediment transport pattern after 200 hours.

The situation after 200 hours of wave action is shown in the right part of Figure 2. From this Figure it can be expected that a tombolo will be formed in the lee of the breakwater. At each breakwater tip a large scour hole develops. The sediment transport pattern after 200 hours is shown in the right part of Figure 4. Due to the formed tombolo in the lee of the breakwater the gyres are migrated towards the exposed area. The same happens to the sediment transport field which in the Bijker formula depends strongly on the flow pattern.

Oblique incident waves

If the waves are arriving at an angle to the shore a wave driven longshore current is present. In the left part of Figure 5 the initial flow field is shown. The longshore current reaches values up to 0.5 m/s. In the lee of the breakwater two gyres are generated but at the up-stream side this gyres is very much smaller and weaker compared to the down-stream gyre. The sediment transport related to this flow field is shown in the middle part of Figure 5. Sediment is trapped into the lee of the breakwater at the up-stream side by the longshore current while erosion occurs at the down-stream breakwater tip due to the strong current velocity of combined gyre and longshore current.
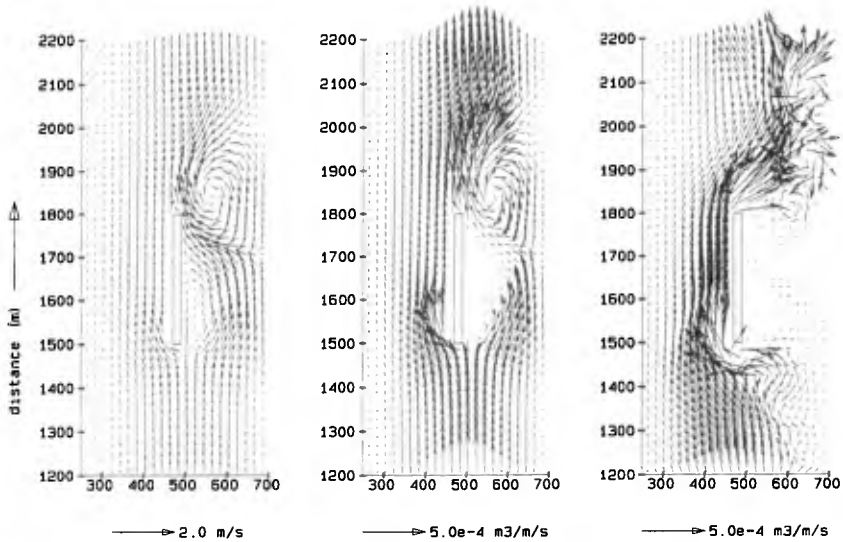
Figure 5 Left: Initial flow pattern; middle: Initial sediment transport pattern; right: Sediment transport pattern after 40 days.

Figure 6 shows the bathymetry after 200 hours and after 40 days respectively. Sediment is trapped into the lee of the breakwater forming a tombolo while a scour hole is generated at the down-stream breakwater tip. However, after some time the up-stream bathymetry is re-shaped by the blocking of the sediment transport resulting in natural by-passing. This is shown in the right part of Figure 5. Almost all sediment passes the breakwater at the seaward side of the breakwater filling the scourhole at the down-stream side which result in a migrating scour hole in down-stream direction.
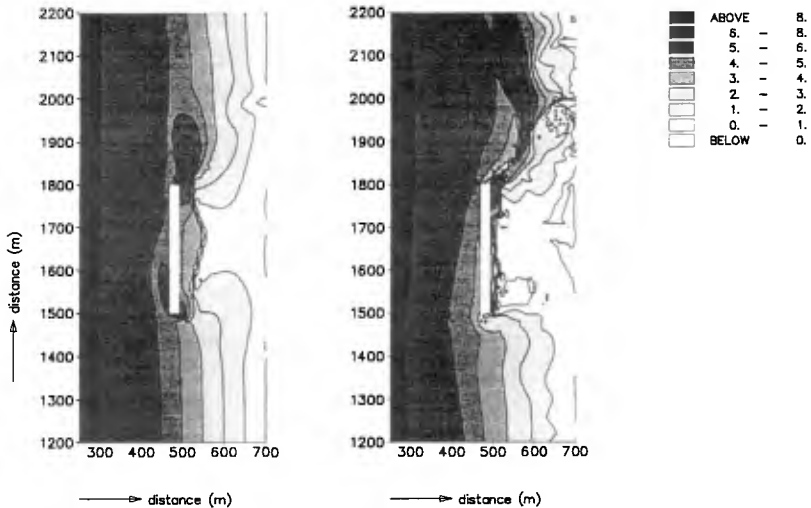

Figure 6 Left: Bathymetry after 200 hours; right: Bathymetry after 40 days.

Finally, the deposition in the lee of the breakwater is shown in Figure 7 for both normal and oblique incident waves.
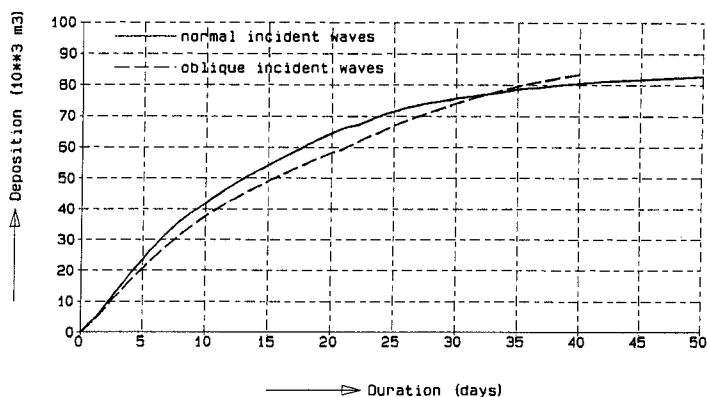

Figure 7 Deposition behind the breakwater.

5. Q3D model

Within the DELFT3D model the transport formula of Van Rijn/Ribberink is used. The transport formula of van Rijn/Ribberink contains a Q3D approach of the nearshore flow pattern. The depth-averaged flow being the result of the TRISULA computation serves as input for a Vertical Structure Model (VSM). This VSM computes the vertical distribution of the horizontal flow velocity components including wind and wave effects and the orbital velocity. The local flow and orbital velocity as computed by the VSM are subsequently used for the prediction of the sediment transport.

Mean current profile

The VSM computes the vertical velocity profile based on the assumption of quasi-steady flow and the assumption that the flow is locally uniform in the horizontal plane. These assumptions follow from the different time and length scales in the nearshore zone. The time and length scales in the vertical plane are much smaller than the time and length scales for the horizontal pattern. Hence, the vertical profile will adjust much faster to changes in external conditions than the horizontal flow pattern.

Primary and secondary current

The description of the primary and secondary current is based on the concept of de Vriend and Stive (1987). Their approach will be outlined in short below.

The current can be split into a primary and a secondary current, according to the definition:

$$u = u_p + u_s \qquad \text{with} \quad u_p = \overline{u}(x,y,t) f_p\left(\frac{z-z_b}{h}\right) \ , \quad \overline{u_s} = 0 \tag{1}$$

with a similar expression for the velocity in y-direction. The suffix p denotes the primary

current, the suffix s the secondary current. From this definition it follows that the depth-averaged flow is determined entirely by the primary current.

After substitution of the definitions for the primary and secondary current into the Reynolds equations for turbulence-averaged flow and integration from the bottom to a point above the highest water surface elevation the primary current can be defined such that:

$$\frac{\partial}{\partial z}\left(v_t \frac{\partial u_p}{\partial z}\right) + \frac{\tau_{bpx}}{\rho_w h} = 0 \tag{2}$$

Here v_t is the turbulence viscosity, τ_{bpx} is the bottom shear stress related to the primary flow, ρ_w is the mass density of water and h is the water depth.

For the secondary current a more complicated expression was found with contributions of different sources. For practical reasons only the secondary flow resulting from the vertical non-uniformity of the wave-induced forces is taken into account. To describe this wave-induced secondary current the water column is divided into three layers:

1. Surface layer, above the wave trough level
2. Middle layer
3. Bottom boundary layer

Next step in their approach was to reduce the description of the surface layer to its effects on the middle and bottom layer. The effects which should be accounted for are wave breaking and mass flux.

The effect of the wave breaking is taken into account by imposing an effective shear stress at the wave trough level. This representing the transfer of momentum across the wave trough level into the flow. This stress is given by:

$$\tau_{wave} = \frac{D_b}{c} \tag{3}$$

in which:

τ_{wave}	=	shear stress at wave through level representing wave breaking
D_b	=	dissipation due to wave breaking
c	=	wave propagation speed

Non-breaking progressing waves cause an onshore mass flux above the wave trough level in the direction of wave propagation. Since there is no net flux this has to be compensated by an averaged velocity at lower levels that is opposite to the wave direction (undertow). The mass flux follows from:

$$m = \frac{E}{c} \tag{4}$$

in which:

m	=	mass flux
E	=	wave energy
c	=	wave propagation velocity

The equation for the wave-induced secondary flow could now be derived from the momentum equation for the middle layer and the expression of the primary flow. After some reduction the equation for the secondary flow in the relatively shallow breaker zone yields:

$$\frac{\partial}{\partial z}\left(\nu_t \frac{\partial u_s}{\partial z}\right) = \frac{\tau_{tsx} - \tau_{bsx}}{\rho_w(z_t - z_b)} \tag{5}$$

In which τ_{tsx} is the effective shear stress at the wave trough level, τ_{bsx} is the bottom shear stress related to the secondary flow, z_t the wave trough level and z_b the bottom level.
Equation 5 can be solved with the integral condition of continuity which yields that the mass flux in the surface layer must be compensated by a return flow in the lower layers:

$$\int_{z_b}^{z_t} u\, dz = -\frac{m}{\rho_w} \tag{6}$$

Eddy viscosity model

Within DELFT3D the mean current profile in the remaining two layers is computed using an eddy viscosity model according to van Rijn et al. (1995). The viscosity is written as the product of a scale factor and a shape function. The distribution of the eddy viscosity is assumed to be parabolic in both layers and zero at $z = 0$.

Since there are different sources which contribute to the turbulence viscosity the VSM distinguished three limit cases for which the combined viscosity must reduce. These cases are:

1. Turbulence viscosity for purely slope-driven currents. In this case the distribution of the eddy viscosity is parabolic and zero at the bottom level and the water surface.
2. Turbulence viscosity for purely wind-driven currents. In this case a maximum is expected near the surface, so the eddy viscosity distribution is taken half-parabolic.
3. Turbulence viscosity generated by wave breaking. The distribution of in this case is assumed to be similar to that induced by wind stress.

Near-bed orbital velocity

The model of the time-variation of the near-bed velocity (orbital motion) is based on the concept described in Roelvink and Stive (1989). They suggested to split this oscillatory part of the near bottom flow, $\tilde{u}$ into a component varying on the time scale of the wave groups, u_l and a component varying on the time scale of the individual waves, u_s.
Assuming that $u_l \ll u_s$ two contributions can be distinguished which contribute to the time-varying flow; non-linear short waves and long waves/short wave interaction. The contribution due to non-linear short waves is computed using Rienecker and Fenton's method (1981) for monochromatic waves while the contribution due to bound long waves is based on Sand (1982), and an empirical relationship for the phase of the bound wave relative to the short wave envelope.

In the transport model of van Rijn/Ribberink a complete representative time-serie of the near-bed velocity is made. This time-serie has the same characteristics of asymmetry, long waves and amplitude modulation. The method followed is outlined in DELFT HYDRAULICS (1995).

Continuity correction

Based on the concept outlined above the test case was applied to the Q3D model. From the first runs it appeared that a lot of sediment was transported by the secondary current in

offshore direction, creating a huge bar (see also left part of Figure 8). This was caused by the return flow which remains constant and at the same location in between full hydrodynamic runs (branch A in the model scheme). Since this enormous bar seems quite unrealistic the number of sediment transport steps was decreased which lead to better results. However, this results in higher computational costs since more hydrodynamic runs has to be carried out. Therefore it was suggested to update the undertow by the continuity corrections.

The secondary current is determined by eq. 5. From this equation it can be seen that the wave breaking-induced shear stress τ_{tsx} at the wave trough level is a very important parameter in the driving of the undertow. This parameter is defined by:

$$\tau_{tsx} = \tau_{wind} + \frac{D_b}{c}$$

(7)

with τ_{wind} is the shear stress at the wave trough level due to wind.

The effect of the decreasing water depth on the undertow can be taken into account by updating the wave energy dissipation D_b after each transport and bottom step. The wave energy dissipation is determined from the dissipation model of Battjes and Janssen (1978):

$$D_b = \frac{1}{4}\rho_w g Q_b \frac{H_{max}}{T_m}$$

(8)

with:

H_{max} = maximum wave height according to Miche criterion
T_m = mean wave period
Q_b = fraction of breaking waves

Updating the wave energy dissipation improves the simulation of the waves breaking on the generated bar and result in a stronger undertow at these particular locations. When the wave action and the undertow are strong enough this will cause the bar to travel further downward the cross-shore profile and reduces the amount of sediment deposited at the same location. The resulting profile development with the improved model is shown in the right part of Figure 8.

It should be noticed that the wave height during the transport and bottom steps still remains constant. Since the wave height is needed to determine the fraction of breaking waves Q_b, the dissipation is still not updated completely.
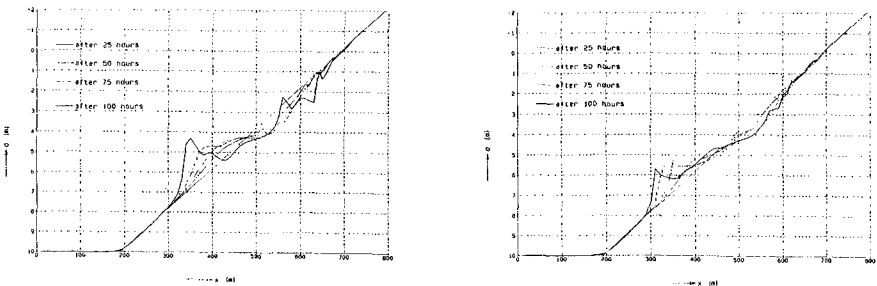

Figure 8 Left: Profile development without updating return flow; right: Profile development with updating return flow.

6. Q3D results

Normal incident waves

Since the hydrodynamic results are the same for both the 2DH and Q3D model here the attention is focused on the sediment transport and bottom changes.

The initial sediment transport pattern is presented in the left part of Figure 9. Sediment is transported by the return flow in offshore direction, while the gyres in the lee of the breakwater transport sediment towards the centre line of the sheltered area. The resulting bathymetry after 100 hours of wave action is shown in the right part of Figure 9. A double salient is generated at the moment while the bottom profile in the exposed area is changed in a similar way as shown in Figure 8. The resulting bathymetry contains very irregular contour lines which affect the progress of the computation (disturbing effect on the flow pattern).
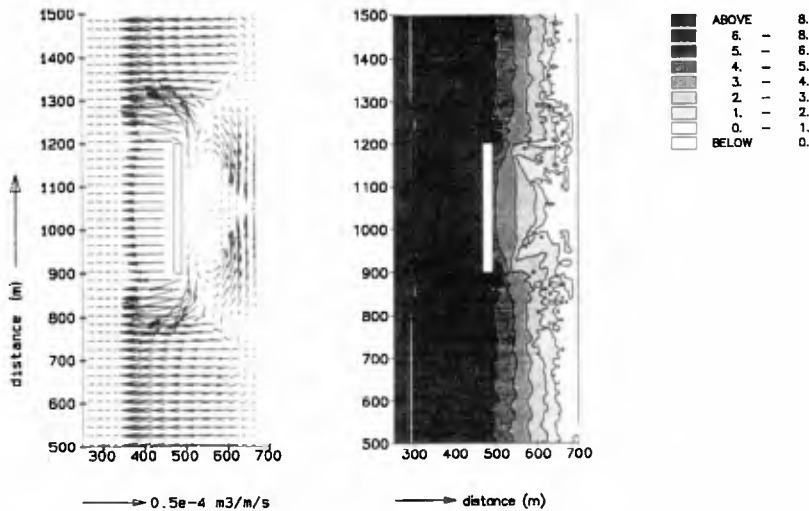
Figure 9 Left: Initial sediment transport pattern; right: Bathymetry after 100 hours.

Oblique incident waves

The initial sediment transport and resulting bathymetry after 100 hours is shown in Figure 9. The sediment transport pattern shows that the cross-shore sediment transport is still dominating over the longshore sediment transport. This seems to be one of the causes of the same irregularities occuring in the bottom contour lines.
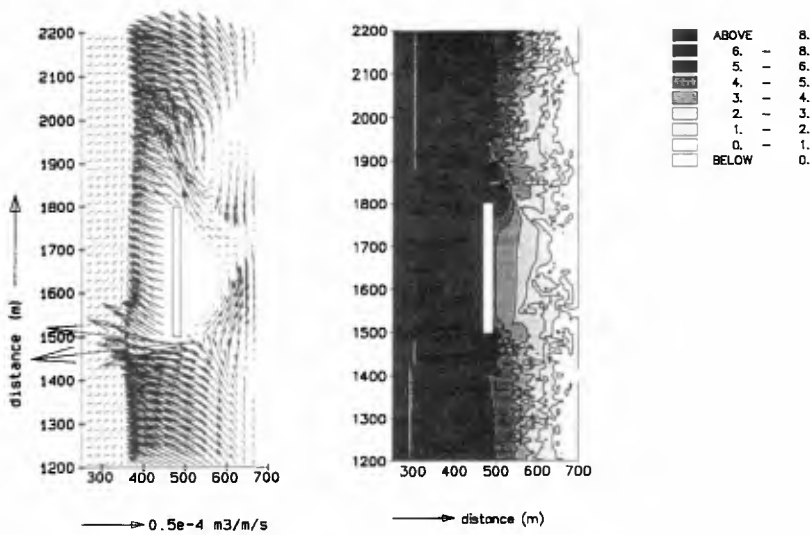
Figure 10 Left: Initial sediment transport pattern; right: Bathymetry after 100 hours.

5. Discussion

In Table 1 criteria for the formation of salients and tombolos, derived from laboratory and field data are given. From this table it can be concluded that most criteria pointed to the formation of a tombolo for the simulated test case. Based on these criteria it can be concluded that the 2DH model results show good qualitative agreement. With this model the equilibrium situation can approximately be simulated.

Reference	Criterion	Present case
Gourlay (1981)	$L_b/X_b \geq 0.67$ Tombolo	$L_b/X_b = 1.36$ Tombolo
Dally and Pope (1986)	$L_b/X_b \leq 0.5$ Salient $L_b/X_b \geq 1.5$ Tombolo	$L_b/X_b = 1.36$ Salient/Tombolo
Harris and Herbich (1986)	$L_b/X_b < 1$ Salient $L_b/X_b > 1$ Tombolo	$L_b/X_b = 1.36$ Tombolo
Suh and Dalrymple (1987)	$L_b/X_b > 1$ Tombolo	$L_b/X_b = 1.36$ Tombolo
Hanson and Kraus (1990)	$L_b/\lambda_b \leq 48(1-K_t)H_0/h_b$ Salient $L_b/\lambda_b \leq 11(1-K_t)H_0/h_b$ Tombolo	$\dfrac{L_b/\lambda_b}{(1-K_t)H_0/h_b} = 1$ Salient
Hsu and Silvester (1990)	$L_b/X_b > 1.33$ Tombolo	$L_b/X_b = 1.36$ Tombolo

Table 1   Criteria for the formation of salients and tombolos (L_b=breakwater length, X_b=breakwater axis-to-shore distance, K_t=transmission of the breakwater, H_0=deep water wave height and λ_b=wave lenght at the breakwater)

The 2DH results with normal incident waves were also compared with other model results by Nicholson et al. (1996). From this comparison it was concluded that the area models are able to reproduce the major morphological features ossociated with offshore breakwaters. However, it also became clear that the choice of the sediment transport formula had a pronounced influence on the resulting morphology. This is also shown within this study by comparison between the sediment transport rates computed with the formula of Bijker and the formula of van Rijn/Ribberink.

Within this study the Q3D model has been improved so that the breakwater test case can be reproduced. From the results it is shown that the sediment transport by the undertow is a dominating feature in the initial state. However, since the prediction of the bathymetry contains very irregular contour lines, the equilibrium state can not be simulated until now.

References

Dally, W.R. and Pope, J., 1986. Detached breakwaters for shore protection. Tech. Report CERC-86-1, U.S. Army Engineer Waterways Experiment Station, Vicksburg, U.S.A.

Delft Hydraulics, 1995. Yearly averaged sediment transport along the Dutch shore. Report H2129.

Gourlay, M.R., 1981. Beach processes in the vicinity of offshore breakwaters. In: Proc. 5th Australian Conference on Coastal and Ocean Engineering, Perth, Australian.

Hanson, H. and Kraus, N.C., 1990. Shoreline response to a single transmissive detached breakwater. In: Proc. 22th International Conference on Coastal Engineering, Delft.

Harris, M.M. and Herbich, J.B., 1986. Effects of breakwaters spacing on sand entrapment. In: Proc. IAHR-Symposium-86 on scale effects in modelling sediment transport phenomena, Toronto, Canada

Holthuijsen L.H., Booij N. and Herbers T.H.C., 1989. A prediction model for stationary, short-crested waves in shallow water with ambient currents. Coastal Engineering, Vol. 13, pp. 23-54, Elsevier.

Hsu J.R.C. and Silvester R., 1990. Accretion behind single offshore breakwater. J. Waterway, Port, Coastal and Ocean Engineering, ASCE, 116(3): 362-380.

Johnson, H., Brøker I. and J.A. Zyserman, 1994. Identification of some relevant processes in coastal morphological modelling. Proc. 24th Int. Conf. on Coastal Engineering, pp. 2871-2885.

Nicholson J., Brøker I., Roelvink J.A., Price D., Tanguy J.M. and Moreno L., 1996. Intercomparison of coastal area morphodynamic models.

Reinecker, M.M. and Fenton, J.D., 1981. A Fourier approximation method for steady water waves. Journal Fluid Mech., Vol. 104, pp. 119-137.

Roelvink, J.A. and G.K.F.M. van Banning, 1994. Design and development of DELFT3D and application to coastal morphodynamics. Proc. Hydroinformatics '94, Balkema, Rotterdam, pp. 451-456.

Roelvink, J.A., D.J.R. Walstra and Z. Chen, 1994. Morphological modelling of Keta Lagoon case. Proc. 24th Int. Conf. on Coastal Engineering, pp. 3223-3236.

Roelvink, J.A. and Stive, M.J.F., 1989. Bar-generating cross-shore flow mechanisms on a beach. Journal of geophysical research, Vol. 94, no. C4, pp.4785-4800.

Reinecker, M.M. and Fenton, J.D., 1981. A Fourier approximation method for steady water waves. Journal Fluid Mech., Vol. 104, pp. 119-137.

Sand, S.E., 1982. Long wave problems in laboratory models. Journal, Waterway, Port, Coastal, and Ocean Engineering, Div. Am. Soc. Civ. Eng., Vol. 108, pp. 492-503.

Suh, K. and Dalrymple, R.A., 1987. Offshore breakwaters in Laboratory and field. Journal, Waterway, Port, Coastal, and Ocean Engineering, Div. Am. Soc. Civ. Eng., Vol. 113,

pp 105-121.

Van Rijn, L.C., Reniers, A., Zitman, T. and Ribberink, J.S., 1995. Yearly-averaged sand transport at the 20 m and 8 m NAP depth contours of the JARKUS-profiles 14, 40, 76 and 103, Report H1887, Delft Hydraulics.

Vriend, H.J. de and Stive, M.J.F., 1987. Quasi-3D modelling of nearshore currents. In: P.P.G. Dyke (ed), JONSMOD'86, Coastal Eng. 11, pp. 565-601.